Ab initio study of pressure-induced metal-insulator transition in cubic FeGe

Matthias Neef,[1] Klaus Doll,[1,2] and Gertrud Zwicknagl[1]
[1]*Institut für Mathematische Physik, TU Braunschweig, Mendelssohnstraße 3, D-38106 Braunschweig, Germany*
[2]*Max-Planck-Institut für Festkörperforschung, Heisenbergstraße 1, D-70569 Stuttgart, Germany*
(Received 15 April 2009; revised manuscript received 25 June 2009; published 20 July 2009)

Ab initio density functional calculations have been performed for cubic FeGe. The calculated equilibrium geometry as well as the ordered magnetic moment in the ground state are in excellent agreement with experiment. To study the influence under pressure, we survey the electronic structure varying the lattice constant while fully relaxing all atomic positions for magnetic and nonmagnetic states. At a critical pressure $p_c \simeq 40$ GPa, the magnetic solution becomes unstable and the ordered magnetic moment disappears. The breakdown of magnetism is associated with the opening of a gap in the electronic density of states which highlights a pressure-induced metal-to-insulator transition. Standard exchange-correlation functionals based on the local density approximation and the generalized gradient approximation (GGA) suggest a continuous decrease in the ordered magnetic moment under pressure. This changes to first order when the nonlocal character of the exchange-interaction is accounted for, with the hybrid functional B3LYP.

DOI: 10.1103/PhysRevB.80.035122 PACS number(s): 71.15.Nc, 71.30.+h, 62.50.−p

I. INTRODUCTION

Structure, electronic properties and magnetism are strongly intertwined in Fe metalloid compounds such as FeSi or FeGe.[1–12] The sensitivity of the electronic and magnetic properties with respect to variations in external fields makes these systems highly interesting for potential applications. Reducing the lattice constants by application of external pressure generally reduces magnetic moments and destabilizes magnetic order.

In the present paper we report theoretical *ab initio* studies of the metal-insulator transition in cubic FeGe, which is metallic at ambient pressure. The central focus is the interplay between structure and magnetism in this material which is an isostructural and isoelectronic analog of the narrow-gap semiconductor FeSi. Bulk FeGe crystallizes in the B20 structure. Two further structures exist at higher temperature: above 620 °C, the cubic B20 structure changes into the hexagonal B35 structure (CoSn type).[13] At 740 °C, a monoclinic high-temperature phase becomes stable, which has the same structure as CoGe.[14] Recently it was shown that the complexity of competing interactions can lead to novel properties in the nanophase.[15]

To better understand the basic mechanisms, which determine the magnetic properties in this material, we investigate the cubic polymorph of FeGe, i.e., the cubic B20 structure which can be viewed as a distorted rock salt structure with four FeGe units in the primitive cell. The lack of inversion symmetry introduces a hierarchy of energy scales, which determines the magnetic structure. This is in close analogy to MnSi where the evolution of the magnetic structure has been studied in detail.[16] First, there is the ferromagnetic exchange interaction between the magnetic moments of $\sim 1\ \mu_B$ per Fe atom[17,18] which favors parallel alignment. This interaction is reflected in the long wavelength of the helical spin structure observed below 279 K. The ferromagnetic alignment is twisted into a helix[19] by the weak Dzyaloshinskii-Moriya interaction which is a consequence of the spin-orbit interaction. Finally, the orientation of the propagation vector is determined by the crystalline electric field. The present calculations focus on the energy scale set by the ferromagnetic exchange. This amounts to approximating the long-wavelength spin spiral by a locally ferromagnetic structure.

In FeGe, a transition from a ferromagnetic metal to a nonmagnetic semiconductor is expected to occur under pressure. This is inferred from recent experiments on the alloy series $FeSi_xGe_{1-x}$ where a metal-insulator transition has been found near $x=0.25$.[20] Assuming that the main effect of the Ge substitution by the smaller Si ion is the reduction of the lattice constant suggests that the transition can be observed also by applying pressure. In fact, FeGe exhibits anomalies in the transport properties under pressure.[21] The magnetic order is strongly suppressed, the system however remains metallic up to the highest pressures investigated so far. Our calculations indicate that the metal-insulator transition should occur at even higher pressures.

A pressure-induced metal-to-insulator transition with the large volume state being the metallic one seems rather unusual at first glance. Upon compression, the overlap of the wave functions at neighboring sites and, concomitantly, the widths of the energy bands are increased which, in turn, reflect the formation of coherent Bloch states. Within bandwidth control, for metal-insulator transition systems the large volume state was expected to be the insulating one (for a review see, e.g., Ref. 22). The electronic structure results show that the pressure-induced metal-to-insulator transition in FeGe is a consequence of the breakdown of magnetism.

We calculate the variation with pressure of the structural, electronic, and magnetic properties of FeGe. This raises the question whether the electrons of the partially filled Fe *d* shells can be treated as itinerant or whether a description in terms of local moments is more appropriate. The issue has been discussed controversially.[1–12,23] We adopt the itinerant picture performing electronic structure calculations within density-functional theory (DFT). This assumption is based on photoemission data for the isoelectronic compound FeSi.[11,24,25] The apparent absence of a Kondo-like feature in the measured single-particle spectral function suggests that FeSi is not a Kondo insulator. In addition, the Fe-3*d* states

exhibit considerable dispersion which is consistently and quantitatively reproduced by an itinerant ansatz.

Band-structure calculations within the local density approximation (LDA) correctly predict FeGe to be a ferromagnetic metal. The ordered magnetic moment in the ground state, however, is underestimated by an order of magnitude. The ordered moment increases with increasing lattice constant.[26] A LDA+U calculation with a value of U =3.7 eV for the local repulsion parameter gave the correct ferromagnetic ground state with a magnetization of $\sim 1\ \mu_B$.[9] A spin-polarized ground state was predicted for FeGe within LDA with a small magnetic moment which increases with increasing the lattice constant.[26] Calculations based on the fixed spin method and using the experimentally determined geometry led to the preference of a ferromagnetic solution.[27] Additionally, a metamagnetic transition from a nonmagnetic semiconductor to a ferromagnetic metal was observed, induced by a magnetic field. This could indicate that the unusual characteristics of FeSi are due to the proximity to a critical point of a transition between semiconducting and ferromagnetic metallic behavior.

In this work, we present calculations based on DFT using different functionals. The choice of the functionals allows for a systematic study of the influence and relative importance of various corrections to the LDA. The latter include gradient corrections and nonlocal exchange. For comparison, we present results derived from the Hartree-Fock (HF) scheme. We study the evolution of the structural, electronic, and magnetic properties with the lattice volume. At a given volume, the optimal structure is determined for every functional by minimizing the total energies for nonmagnetic and spin-polarized states. The magnetic moment in the ground state for a given functional and given volume/lattice constant is finally derived by comparing the energies for the nonmagnetic and spin-polarized solutions. The pressure dependence of the properties is derived from the enthalpy.

The paper is organized as follows: In Sec. II we describe the computational method. The results for the ground state and the metal to semiconductor transition are discussed in Secs. III and IV. Section V gives the concluding remarks and suggestions for experiments.

II. METHOD

First-principles electronic structure results reported in the present paper were obtained by the code CRYSTAL.[28] Exchange and correlation were introduced using various density functionals as well as the Hartree-Fock approximation. The density functionals include the Perdew-Zunger parametrization of the Ceperley-Alder data[29] and the gradient-corrected Perdew-Wang functional,[30] hereafter referred to as LDA and PW91, respectively. Of particular interest is the hybrid functional B3LYP which allows to incorporate nonlocal exchange (see, e.g., Ref. 31). A sampling net with $16\times16\times16$ **k** points in the Brillouin zone was used, and a smearing temperature of 0.136 eV was applied to facilitate the numerical integration.

We used the experimentally established B20 structure in which the crystallographic unit cell contains four germanium and four iron atoms. The experimental values for the lattice constant and the internal coordinates at ambient pressure are a=4.70 Å and u_{Fe}=0.1352, u_{Ge}=0.8414.[14] The latter indicate significant deviations from the rock salt structure which is characterized by u_{Fe}=0.25, u_{Ge}=0.75. In the B20 structure, the point symmetry at the Fe or Ge sites is C_3. The Fe ion has seven Ge neighbors whose distances depend on the internal coordinates. The nearest Ge atom is at a distance of 2.391 Å three Ge atoms are at a distance of 2.443 Å, and three Ge atoms are at a distance of 2.646 Å.

TABLE I. Optimized diffuse exponents of the basis functions.

	Fe			Ge	
	sp	*sp*	*d*	*sp*	*d*
LDA	0.53	0.10	0.26	0.18	0.65
GGA	0.52	0.10	0.26	0.18	0.61
B3LYP	0.52	0.10	0.26	0.18	0.71
HF	0.52	0.15	0.29	0.14	0.95

For a given exchange-correlation functional, we chose a set of Gaussian-type orbitals centered at the position of the atoms. An iron atom has an occupancy of $1s^2 2s^2 2p^6 3s^2 3p^6 4s^2 3d^6$. To describe this, a basis set with four s, two p, and one d function would be sufficient which would be labeled as $[4s2p1d]$. This would however only correspond to a minimal basis set. It is better to have a larger basis set which offers more flexibility, in order to describe the chemical bond and so on. Similarly, a germanium atom has an $1s^2 2s^2 2p^6 3s^2 3p^6 3d^{10} 4s^2 4p^2$ occupancy, and a minimal basis set would thus correspond to the size $[4s3p1d]$. Again, one usually chooses a larger basis set in order to have more flexibility. An introduction to the quantum chemical methods and basis set notation can be found, e.g., in the textbook by Szabo and Ostlund.[32]

The present all electron calculations use a $[6s5p2d]$ basis at the Fe site where the inner $[4s3p1d]$ basis functions were chosen as in Ref. 33. Two diffuse sp shells and a diffuse d shell were added and optimized. The Ge $[5s4p2d]$ basis set was taken from Ref. 34. The diffuse exponents were reoptimized so as to minimize the total energy of nonmagnetic FeGe in a hypothetical rock salt structure. The higher-symmetric NaCl was chosen as this reduces the required computing time for this step considerably. The reliability of the computational method had been tested for the case of FeSi. A detailed discussion is given in Ref. 10. The HF calculations were performed with a slightly modified inner d shell for the Ge atom: to avoid convergence problems, the smallest d exponent (0.9404) of the first contraction of the Ge basis set was eliminated.

The results for the optimized diffuse exponents are given in Table I. The electronic properties depend rather sensitively on the detailed structure. For all effective single-particle models (HF, LDA, PW91, and B3LYP), the internal coordinates were optimized using analytical gradients[35–37] for various volumes, in order to determine the energy as a function of the volume.

TABLE II. Results of the geometry optimization for the spin polarized solution, for various methods. The lattice constant a and the internal coordinates of iron u_{Fe} and of germanium u_{Ge} were optimized. In addition, the bulk modulus B is displayed.

	a (Å)	u_{Fe}	u_{Ge}	B (GPa)
LDA	4.54	0.137	0.840	223
PW91	4.66	0.136	0.842	176
B3LYP	4.83	0.132	0.844	110
Experiment	4.70[a]	0.1352[a]	0.8414[a]	147[b]

[a]Reference 14
[b]Reference 21

III. ELECTRONIC STRUCTURE

The exchange-correlation functionals considered here yield a magnetic ground state in agreement with experiment. The results of the calculated equilibrium structures are summarized in Table II. The lattice constants, internal coordinates and bulk moduli agree reasonably with experiment. There are, however, characteristic discrepancies. The LDA overestimates the binding energy which is reflected in a relatively short lattice constant and a high-bulk modulus. The nonlocal exchange, on the other hand, reduces the binding energy which results in a larger lattice constant and small bulk modulus. Assuming a magnetic ground state we find no equilibrium structure within the HF approximation. Expanding the lattice constants up to a value of $a=5.30$ Å lowers the total energy monotonously. When the lattice constants were further increased, the self-consistency equations could not be converged.

The covalent character of the bond is reflected in the small charge transfer of $\sim 0.7|e|$ which is obtained from all density functionals (see Table III). This value is slightly larger than the one of $\sim 0.4-0.6|e|$ which was found with the same functionals in the case of FeSi.[10] A further indication of covalency is the overlap population between Fe and the neighboring Ge of ~ 0.2, which is comparable to FeSi.[10]

While the values for the total charge transfer agree for the functionals chosen, there are nevertheless discrepancies concerning the orbital character of the occupied single-electron states. As mentioned above, the admixture of the nonlocal exchange in the B3LYP-functional leads to a larger lattice constant and a smaller occupation of the Fe d orbitals bringing the system closer to the atomic d (Ref. 6) configuration. Due to the stronger localization it is energetically more favorable to occupy the states with a larger magnetization as compared to the LDA and the PW91 functional. A further difference is the occupation of the d orbitals with the B3LYP functional. The occupancy of the d_{xy}, d_{xz}, and d_{yz} orbitals is $\sim 1.5|e|$ each, while that of the d_{z^2} and $d_{x^2-y^2}$ orbitals is $\sim 1.2|e|$. The spin population is ~ 0.7 in d_{xy}, d_{xz}, d_{yz}, and ~ 0.4 in the d_{z^2} and $d_{x^2-y^2}$ orbitals (note that a spin population of 1.0 corresponds to spin $\frac{1}{2}$). For the LDA and the PW91 functionals, the occupancies are approximately equal for all the d orbitals (population $\sim 1.4|e|$, spin population ~ 0.04).

TABLE III. Charge at the Iron and Germanium site of ferromagnetic FeGe in the B20 structure calculated with the Mulliken population analysis. The total charge (Fe total and Ge total), and the projected charge (Fe d and Fe sp) are shown. The analysis was performed with the optimized geometry of the spin-polarized calculation in Table II.

	Fe sp ($\|e\|$)	Fe d ($\|e\|$)	Fe total ($\|e\|$)	Ge total ($\|e\|$)
LDA	19.58	7.18	26.76	31.24
PW91	19.63	7.10	26.73	31.27
B3LYP	19.78	6.92	26.70	31.30

TABLE IV. Results of the geometry optimization for the nonmagnetic solution. The lattice constant a and the internal coordinates u_{Fe} and u_{Ge} were optimized. The bulk modulus B and the indirect gap Δ_{ind} are displayed.

	a (Å)	u_{Fe}	u_{Ge}	Δ_{ind} (eV)	B (GPa)
LDA	4.54	0.137	0.840	0.088	238
PW91	4.64	0.135	0.840	0.104	195
B3LYP	4.63	0.134	0.838	1.401	201
HF	5.15	0.167	0.828	1.468	33

Let us now consider the nonmagnetic reference state which is energetically less favorable at ambient pressure. The structure data summarized in Table IV show that the LDA and PW91 results are rather insensitive to the magnetic order. The B3LYP lattice constant, on the other hand, is strongly reduced in the nonmagnetic state. When spin-polarization is suppressed, a stable HF solution can be found.

We next turn to the magnetic properties of the ground state at ambient pressure which are summarized in Table V. All quantities are evaluated using the optimized geometry of the corresponding exchange-correlation functional. The energy gain due to magnetic order and the ground state magnetization strongly depend on the functional. The LDA predicts a very small ordered moment in the ground state which corresponds to a very small energy gain E_{FM-NM} due to spin polarization. Here E_{FM-NM} denotes the difference between the ferromagnetic ground state and a hypothetical nonmagnetic state with the same lattice constant. The experimentally

TABLE V. Magnetic properties of ferromagnetic FeGe in the B20 structure. The total and individual (Iron and Germanium) magnetization M per one formula unit are displayed. The energy difference between the magnetic and the nonmagnetic solution E_{FM-NM} is for one formula unit.

	M (μ_B)	M_{Fe} (μ_B)	M_{Ge} (μ_B)	E_{FM-NM} (eV)
LDA	0.16	0.17	−0.01	−0.0003
PW91	1.00	1.10	−0.11	−0.047
B3LYP	2.30	2.51	−0.21	−0.67
Experiment	1.00[a]			

[a]Reference 18

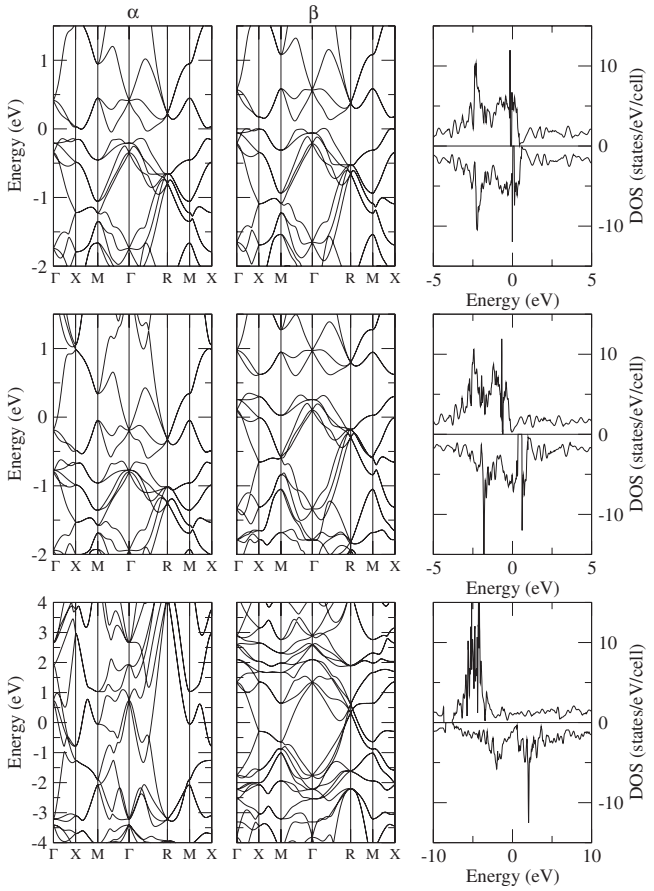

FIG. 1. Band structure and DOS of ferromagnetic FeGe in B20 structure using the (a) LDA, (b) PW91, and (c) B3LYP exchange-correlation functional. The energy bands were calculated for the optimized structures as described in Table V. Majority and minority bands are labeled with the spin indices α and β, respectively.

determined magnetization of 1 μ_B per Fe atom agrees best with the magnetic moment obtained from PW91. With the PW91 functional, there is also a larger energy difference between magnetic and nonmagnetic solution. The largest magnetization is obtained for B3LYP. These findings can be understood as follows. The small ordered moment predicted by the LDA is a consequence of the small lattice constant. At the experimental lattice constant of a=4.70 Å the ordered magnetic moment computed within LDA reaches the observed value of 1 μ_B per Fe atom. The increase in magnetic moment with increasing lattice constant is similar to what was observed in an earlier LDA calculation.[26] The Fe d states are more localized in the B3LYP ground state than they are in LDA and PW91. This is a consequence of the nonlocal exchange. As a result, double occupancy of these orbitals becomes energetically less favorable which, in turn, reduces their contribution to binding as reflected in the large volume, and enhances the magnetic moment.

The differences concerning geometry and charge distribution are reflected in the band structure and the density of states (DOS) as can be seen from Fig. 1. For LDA, the dispersion of the majority and minority bands is similar. The main difference is a rigid shift corresponding to an exchange splitting of ~0.14 eV which, in turn, yields the small magnetization. For PW91, the exchange splitting reaches ~0.85 eV which is clearly seen in Fig. 1. In addition, the shape of the unoccupied bands is slightly changed. The fact that the magnetic order mainly results in rigid shifts of majority and minority bands close to the Fermi level is related to the fact that the states have predominantly d character. The same characteristic dispersion is also found for the hypothetical nonmagnetic state in Fig. 2 which closely parallels that of FeSi.[10]

The states at the Fermi level derived from the hybrid functional B3LYP, on the other hand, have significant admixture of Ge sp states. The internal magnetic field set up by the ferromagnetic polarization leads to a significant distortion of the bands. In the hypothetical nonmagnetic reference system, the occupied states are separated by a narrow indirect gap from their unoccupied counterparts. This can be seen from Fig. 2. The nonmagnetic reference system turns out to be a narrow-gap semiconductor. This comparison suggests that the metallic character of FeGe at ambient pressure results from the band shifts associated with the magnetic polarization. For this reason we expect a pressure-induced metal-insulator transition following the suppression of magnetism.

IV. PRESSURE-INDUCED METAL-INSULATOR TRANSITION

The isostructural and isoelectronic counterpart FeSi can be viewed as a compressed and concomitantly nonmagnetic analog of FeGe. Whether or not the properties of FeSi can be explained with a simple band structure calculation or not, is still under discussion. Recently, it was pointed out that photoemission results can essentially be explained with a simple LDA band structure.[11,24,25] Similarly, the infrared spectrum can very well be reproduced on the LDA level.[12] It was even suggested that the unusually shaped susceptibility could be explained by taking into account phonons in an LDA calculation.[38] GGA results are qualitatively similar to LDA. With B3LYP, a low-lying magnetic state was found; but on the other hand B3LYP was not able to reproduce the small gap.[10]

The variation with lattice constant of the total energies for the nonmagnetic and magnetic states is displayed in Fig. 3. Within HF the magnetic solution turns out to be the stable one over the entire range of lattice constants considered here. The DFT total energy curves for polarized states and their unpolarized counterparts, on the other hand, intersect which highlights the suppression of magnetism by pressure.

The critical values of the lattice constant, a_c, are indicated in Fig. 3. The critical volume reduction $\overline{\delta V}_c = \frac{V_0 - V_c}{V_0}$ where V_0 and V_c denote the equilibrium volume and the critical volume, respectively, depends upon the exchange correlation functional. The differences reflect the general trends seen in Table V. As the energy gain due to ferromagnetic alignment is rather small within LDA, a rather small volume reduction $\overline{\delta V}_c \sim 3\%$ is required to render the system nonmagnetic. This corresponds to a pressure of less than 10 GPa at the phase transition (the exact value is difficult to determine due to the small energy and enthalpy difference, at the LDA level). The PW91 and B3LYP functional predict $\overline{\delta V}_c \sim 17\%$ and $\overline{\delta V}_c$

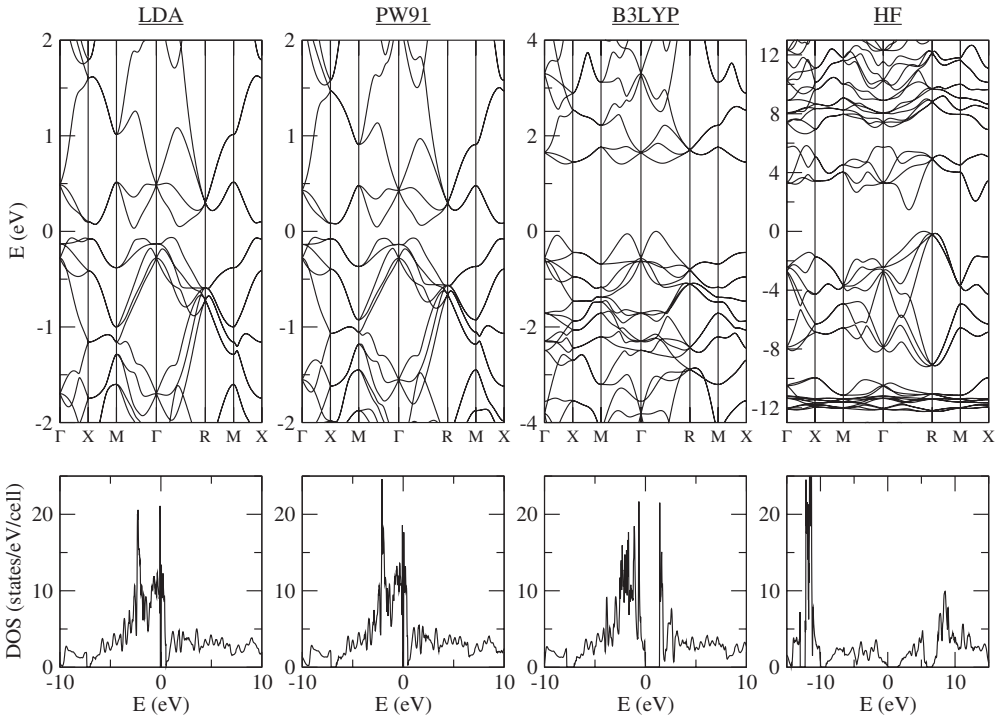

FIG. 2. Band structure and DOS of hypothetical nonmagnetic FeGe in B20 structure using the (a) LDA, (b) PW91, and (c) B3LYP exchange-correlation functionals as well as (d) the HF approximation. The energy bands were calculated for the optimized structures as described in Table IV. The different schemes consistently predict an insulating ground state. The magnitude of the excitation gap depends upon the approximation scheme for electron interaction (see Table IV). All energies are measured relative to the top of the valence band.

~30%, respectively, which corresponds to pressures of 40 GPa (PW91) or 35 GPa (B3LYP). The pressure values are summarized in Table VI. The different volume reductions necessary for the transition are due to the different equilibrium constants of the procedures, because the transition arises with all DFT procedures within the range from 4.4 to 4.5 Å. These values are close to the computed FeSi lattice constant.[10] This is in reasonable agreement with the finding that the metal-insulator transition is at $x=0.25$ for $FeSi_xGe_{1-x}$,[20] i.e., the lattice constant should be close to the one of pure FeSi. The comparison should be taken with a grain of salt, as disorder may also play a role in the case of $FeSi_xGe_{1-x}$. The computed value for the volume at the metal-insulator transition agrees very well with a recent calculation[21] where a volume of 92 $Å^3$ was found, if no zero-point vibrations were included.

Let us consider the transition in greater detail. For LDA and PW91 the slope of the total energy and the magnetization vary continuously across the transition which is therefore classified as a second order transition. Within B3LYP, on the other hand, the properties change abruptly indicating a first order transition. These differences are due to the nonlocal exchange which leads to the formation of metastable magnetic states in the compressed lattice. The nonlocal exchange included in B3LYP favors magnetic states which are distinctly different from the nonmagnetic solutions. This is reflected in the variation with lattice constant of the internal coordinates u_{Fe} and u_{Ge} displayed in Fig. 5. Within LDA and PW91, on the other hand, the nonmagnetic structure continuously evolves out of the magnetic ground state.

TABLE VI. The pressure at the metal-insulator transition, computed with various functionals.

	p (GPa)
LDA	≤10
PW91	40
B3LYP	35

At the metal-insulator transition where the ordered magnetic moment disappears, the system becomes insulating. An analysis of the density of states for lattice constants close to the transition (Fig. 4) shows that up and down bands are shifted in opposite directions. This can be understood within the Stoner model. Due to the exchange splitting, i.e., the relative shift of the bands, no gap exists in the ground state at the computed equilibrium lattice constant (and also at the experimental lattice constant). With increasing pressure, the splitting between majority and minority bands decreases and finally vanishes. At this point, a gap appears in the DOS and the system becomes insulating. The suppression of the exchange splitting and thus the disappearance of magnetism is the cause of the metal-insulator transition with applied pressure. With the PW91 functional, the situation is similar to the LDA, only the two spin channels are stronger deformed.

A qualitative explanation can be given as follows: In the extreme case of free atoms, Hund's rules apply and magnetic atoms exist. Hund's rules are still dominant at large lattice constant, and a magnetic solution is preferable. However, when the lattice constant is reduced, the bandwidths become

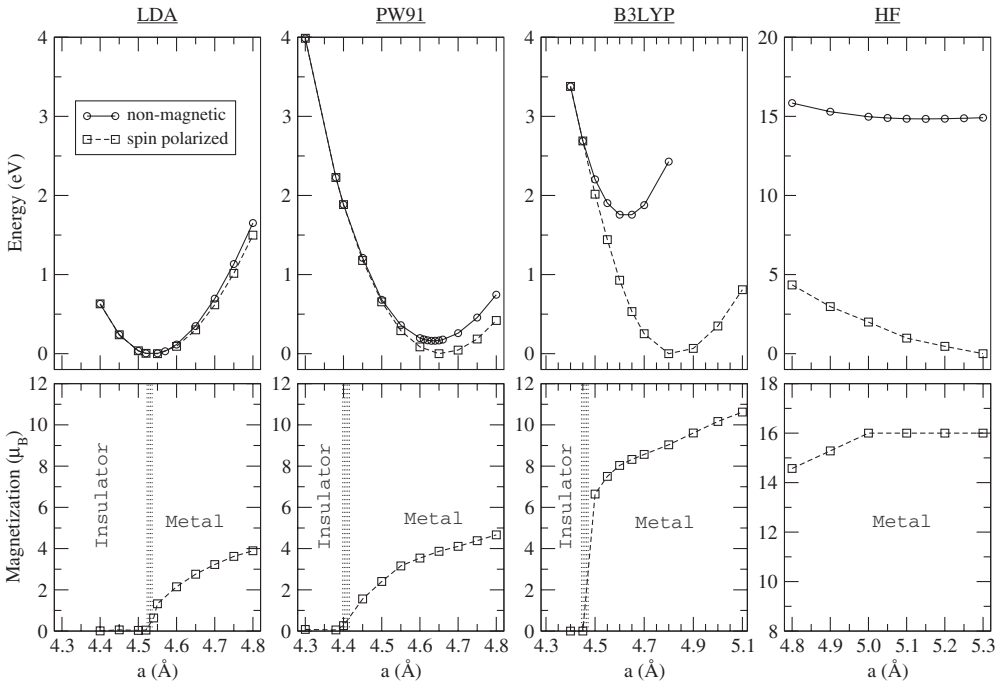

FIG. 3. Upper panel: Total energy vs lattice constant of magnetic (squares) and nonmagnetic (circles) FeGe in B20 structure using LDA, PW91, and B3PYP exchange-correlation functional as well as the HF approximation. For a given value of the lattice constant a the corresponding optimized internal coordinates were used. Lower panel: Variation with lattice constant of the ground state magnetization predicted by LDA, PW91, B3LYP, and HF. The transition from the nonmagnetic state to the magnetic state is indicated. The disappearance of ferromagnetic order is connected with a metal-insulator transition. Note that the data for total energy and magnetization refers to 4 formula units.

larger and larger, and the relative importance of the Coulomb repulsion diminishes, and instead, double occupancy and thus a solution with reduced magnetic moment become favorable. With increasing pressure and thus reduced lattice constant, the magnetic moment becomes smaller and smaller. As an iron atom has four unpaired and a germanium atom four valence electrons, a nonmagnetic and insulating state is possible and becomes the preferred one at high pressure.

The nonlocal exchange included in B3LYP favors magnetic states which are distinctly different from the nonmagnetic solutions. This is reflected in the variation with lattice constant of the internal coordinates u_{Fe} and u_{Ge} displayed in Fig. 5. Within LDA and PW91, on the other hand, the nonmagnetic structure continuously evolves out of the magnetic ground state.

This abrupt change in the geometry at the metal-insulator transition is reflected in the interatomic distances obtained for the magnetic and the nonmagnetic solution within B3LYP (see Fig. 6). The coordinate d_2, i.e., the distance between Fe and the next nearest Ge neighbor changes discontinuously at the critical pressure of $\sim$35 GPa. This is not the case for LDA and PW91.

Experimentally, the helical magnetic order in FeGe is suppressed with a pressure of 19 GPa.[21] The metallic state, al-

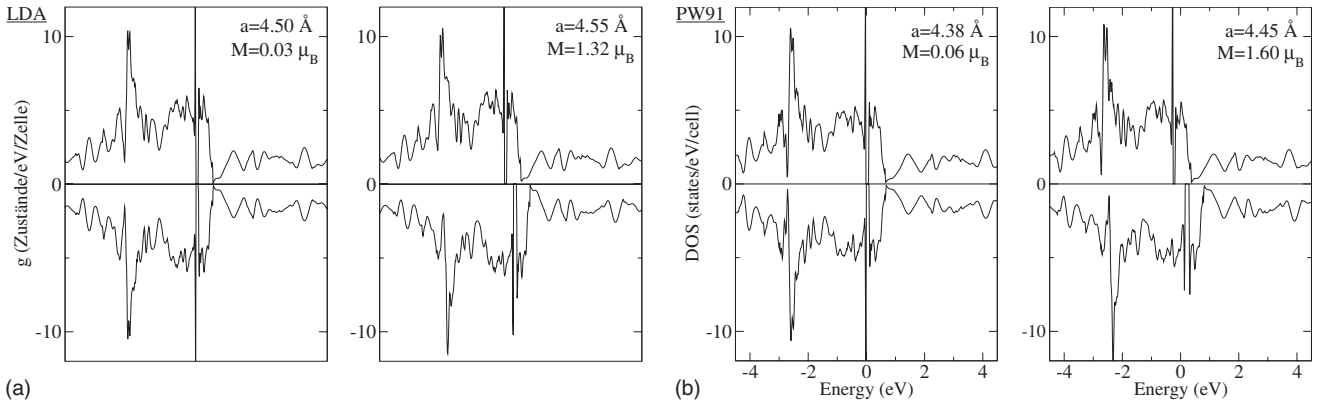

FIG. 4. Evolution of the DOS of FeGe across the magnetic transition for LDA (a) and PW91 (b). The data refer to the results for two values of the lattice constants in the nonmagnetic regime [displayed left in (a),(b)] and the magnetic regime [displayed right in (a),(b)], respectively.

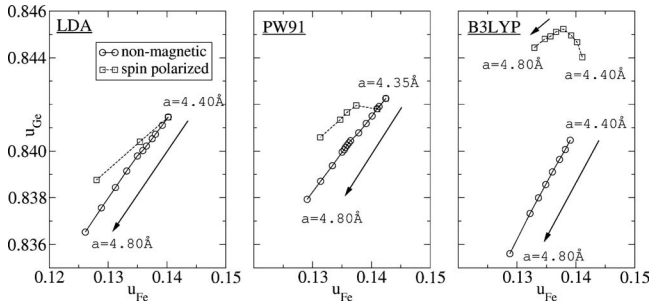

FIG. 5. Variation with lattice constant of the internal coordinates for nonmagnetic states (circles) and magnetic states (squares). The coordinates of each data point visualize the pair of internal coordinates (u_{Fe}, u_{Ge}) derived from minimizing the total energy at a given lattice constant. Following the directions indicated by the arrows, the values of the lattice constant increases from a minimal value a_{min} where the nonmagnetic state is stable across the critical value a_c to a maximum value a_{max} corresponding to a magnetic ground state. For LDA and PW91 the magnetic and nonmagnetic structures coalesce at the critical point. Within B3LYP the magnetic and nonmagnetic structures differ distinctly.

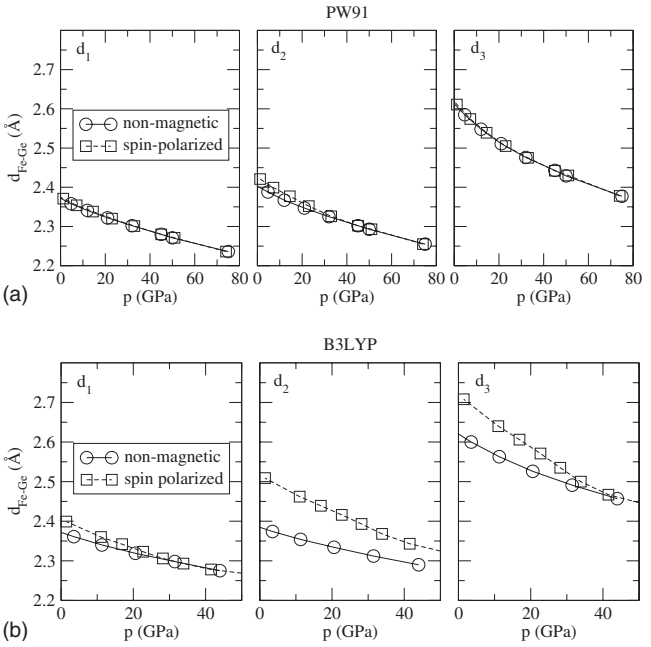

FIG. 6. Variation with pressure of the interatomic distances $d_{\mathrm{Fe\text{-}Ge}}$ between Fe and its nearest (d_1), next nearest (d_2) and third nearest (d_3) Ge neighbor for spin polarized (squares) and nonmagnetic (circles) geometry calculated with the PW91 and the B3LYP functional. The pressure is derived by differentiating the total energy with respect to the volume.

though with unusual characteristics, remains up to pressure of 23 GPa. A discontinuous change in the nearest Fe-Ge distance d_1 was measured, whereas the distances d_2 and d_3 change smoothly. The phase diagram was determined up to 25 GPa. The Röntgen powder-diffraction measurements display that the nearest distance d_1 between iron and germanium is not continuous in the pressure range of 12–15 GPa, at low temperature. The result for d_1 agrees reasonably well with the computed values in Fig. 6; however, d_1 changes continuously in the calculations.

V. CONCLUSION

The system FeGe and a pressure driven metal-insulator transition was studied with various functionals. When pressure is applied, the magnetic moment is reduced and finally becomes zero. With the vanishing of the magnetic moment, the system becomes insulating, and the band structure becomes very similar to that of the related system FeSi. This metal-insulator transition is somewhat different from the usual mechanism, as normally an insulator becomes metallic when pressure is applied. At the level of the local density approximation and the gradient corrected PW91 functional, the metal-insulator transition is continuous and thus of second order. The hybrid functional B3LYP instead predicts a discontinuous transition: the magnetization changes strongly at the metal-insulator transition, and in addition the internal coordinates and thus also some of the interatomic distances change discontinuously. Properties such as the equilibrium lattice constant and the magnetic moment at zero pressure are best described with the PW91 functional. This functional predicts a metal-insulator transition at a pressure value of 40 GPa, and we therefore suggest experiments in this pressure range.

[1] V. Jaccarino, G. K. Wertheim, H. J. Wernick, L. R. Walker, and S. Arajs, Phys. Rev. **160**, 476 (1967).
[2] Z. Schlesinger, Z. Fisk, H.-T. Zhang, M. B. Maple, J. F. DiTusa, and G. Aeppli, Phys. Rev. Lett. **71**, 1748 (1993).
[3] M. Fäth, J. Aarts, A. A. Menovsky, G. J. Nieuwenhuys, and J. A. Mydosh, Phys. Rev. B **58**, 15483 (1998).
[4] D. Mandrus, J. L. Sarrao, A. Migliori, J. D. Thompson, and Z. Fisk, Phys. Rev. B **51**, 4763 (1995).
[5] L. F. Mattheiss and D. R. Hamann, Phys. Rev. B **47**, 13114 (1993).
[6] H. Ohta, S. Kimura, E. Kulatov, S. V. Halilov, T. Nanba, and M. Motokawa, J. Magn. Magn. Mater. **140-144**, 121 (1995).
[7] V. I. Anisimov, S. Y. Ezhov, I. S. Elfimov, I. V. Solovyev, and T. M. Rice, Phys. Rev. Lett. **76**, 1735 (1996).
[8] T. Jarlborg, Phys. Rev. Lett. **77**, 3693 (1996).
[9] V. I. Anisimov, R. Hlubina, M. A. Korotin, V. V. Mazurenko, T. M. Rice, A. O. Shorikov, and M. Sigrist, Phys. Rev. Lett. **89**, 257203 (2002).
[10] M. Neef, K. Doll, and G. Zwicknagl, J. Phys.: Condens. Matter **18**, 7437 (2006).
[11] D. Zur, D. Menzel, I. Jursic, J. Schoenes, L. Patthey, M. Neef, K. Doll, and G. Zwicknagl, Phys. Rev. B **75**, 165103 (2007).
[12] A. M. Racu, D. Menzel, J. Schoenes, and K. Doll, Phys. Rev. B **76**, 115103 (2007).

[13] T. Ohoyama, K. Kanematsu, and K. Yasukochi, J. Phys. Soc. Jpn. **18**, 589 (1963).
[14] M. Richardson, Acta Chem. Scand. **21**, 753 (1967).
[15] C. Zeng, P. R. C. Kent, M. Varela, M. Eisenbach, G. M. Stocks, M. Torija, J. Shen, and H. H. Weitering, Phys. Rev. Lett. **96**, 127201 (2006).
[16] M. L. Plumer, J. Phys.: Condens. Matter **2**, 7503 (1990).
[17] L. Lundgren, K. Å. Blom, and O. Beckman, Phys. Lett. **28A**, 175 (1968).
[18] R. Wäppling and L. Häggström, Phys. Lett. **28A**, 173 (1968).
[19] B. Lebech, J. Bernhard, and T. Freltoft, J. Phys.: Condens. Matter **1**, 6105 (1989).
[20] S. Yeo, S. Nakatsuji, A. D. Bianchi, P. Schlottmann, Z. Fisk, L. Balicas, P. A. Stampe, and R. J. Kennedy, Phys. Rev. Lett. **91**, 046401 (2003).
[21] P. Pedrazzini, H. Wilhelm, D. Jaccard, T. Jarlborg, M. Schmidt, M. Hanfland, L. Akselrud, H. Q. Yuan, U. Schwarz, Y. Grin, and F. Steglich, Phys. Rev. Lett. **98**, 047204 (2007).
[22] Y. T. M. Imada and A. Fujimori, Rev. Mod. Phys. **70**, 1039 (1998).
[23] J. Kunes and V. I. Anisimov, Phys. Rev. B **78**, 033109 (2008).
[24] M. Klein, D. Zur, D. Menzel, J. Schoenes, K. Doll, J. Röder, and F. Reinert, Phys. Rev. Lett. **101**, 046406 (2008).
[25] M. Klein, D. Menzel, K. Doll, M. Neef, D. Zur, I. Jursic, J. Schoenes, and F. Reinert, New J. Phys. **11**, 023026 (2009).
[26] T. Jarlborg, J. Magn. Magn. Mater. **283**, 238 (2004).
[27] H. Yamada, K. Terao, H. Ohta, and E. Kulatov, Physica B **329-333**, 1131 (2003).
[28] R. Dovesi, V. R. Saunders, C. Roetti, R. Orlando, C. M. Zicovich-Wilson, F. Pascale, B. Civalleri, K. Doll, N. M. Harrison, I. J. Bush, P. D'Arco, and M. Llunell, CRYSTAL 2006 *User's Manual* (University of Torino, Torino, 2006).
[29] J. P. Perdew and A. Zunger, Phys. Rev. B **23**, 5048 (1981).
[30] J. P. Perdew, J. A. Chevary, S. H. Vosko, K. A. Jackson, M. R. Pederson, D. J. Singh, and C. Fiolhais, Phys. Rev. B **46**, 6671 (1992).
[31] K. Raghavachari, Theor. Chem. Acc. **103**, 361 (2000).
[32] A. Szabo and N. S. Ostlund, *Modern Quantum Chemistry* (McGraw-Hill, New York, 1989).
[33] G. Valerio, M. Catti, R. Dovesi, and R. Orlando, Phys. Rev. B **52**, 2422 (1995).
[34] E. Ruiz, M. Llunell, and P. Alemany, J. Solid State Chem. **176**, 400 (2003).
[35] K. Doll, V. R. Saunders, and N. M. Harrison, Int. J. Quantum Chem. **82**, 1 (2001).
[36] K. Doll, Comput. Phys. Commun. **137**, 74 (2001).
[37] B. Civalleri, P. D'Arco, R. Orlando, V. R. Saunders, and R. Dovesi, Chem. Phys. Lett. **348**, 131 (2001).
[38] T. Jarlborg, Phys. Rev. B **59**, 15002 (1999).